University of Nebraska - Lincoln
DigitalCommons@University of Nebraska - Lincoln

John R. Hardy Papers | Research Papers in Physics and Astronomy

1-1-1980

Theoretical Lattice-Dynamical Studies of the Incommensurate Phase Transformation in K_2SeO_4

M. S. Haque
University of Nebraska - Lincoln

John R. Hardy
University of Nebraska - Lincoln

Follow this and additional works at: http://digitalcommons.unl.edu/physicshardy

Part of the Physics Commons

Haque, M. S. and Hardy, John R., "Theoretical Lattice-Dynamical Studies of the Incommensurate Phase Transformation in K_2SeO_4" (1980). *John R. Hardy Papers.* Paper 44.
http://digitalcommons.unl.edu/physicshardy/44

This Article is brought to you for free and open access by the Research Papers in Physics and Astronomy at DigitalCommons@University of Nebraska - Lincoln. It has been accepted for inclusion in John R. Hardy Papers by an authorized administrator of DigitalCommons@University of Nebraska - Lincoln.

Theoretical lattice-dynamical studies of the incommensurate phase transformation in K_2SeO_4

M. S. Haque* and J. R. Hardy†
Behlen Laboratory of Physics, University of Nebraska, Lincoln, Nebraska 68588
(Received 7 May 1979)

We have made detailed lattice-dynamical studies of the origin of the incommensurate phase transition in potassium selenate. These were based on a rigid-ion model with Coulomb interactions, and also short-range interactions between restricted numbers of close neighbors. The associated short-range force constants were determined using the static equilibrium conditions for the crystal and the observed Raman frequencies. The calculations were made for the room-temperature structure using the quasiharmonic approximation in which the effects of varying temperature were simulated by varying the short-range force constants. In this way we were able to show that the crystal has a low-frequency optic branch of Σ_2 symmetry which displays softening and instability for wave vectors $\vec{q}$ in the vicinity of $\vec{q}=0.3\vec{a}^*$ where $\vec{a}^*$ is the first reciprocal-lattice vector along the [100] direction. This is in agreement with experimental neutron scattering results and implies a transition to an incommensurate phase. Full sets of dispersion curves at 130 K for the [100] direction are presented. We also present comparisons of the calculated and experimental low-frequency Σ_2 and Σ_3 branches at 130, 145, and 250 K. We show, by decomposition of the squares of the normal-mode frequencies into a sum of Coulomb and short-range components, that the balance between these two kinds of interatomic forces is very delicate. This decomposition also shows that a transition to an incommensurate phase is very likely for both the selenate and isomorphous structures. Our model also enables us to predict that uniaxial stress will rapidly depress the transition temperature; a result also in accord with experiment.

I. INTRODUCTION

In a recent publication[1] we have presented preliminary results of a joint experimental and theoretical investigation on the stress dependence of the transition temperature (T_c) for the structural instability in potassium selenate (K_2SeO_4). In this paper we report a detailed theoretical study of the lattice dynamics of this crystal, with particular emphasis on the behavior of the soft mode which causes the structural phase transition at 130 K.

Structural instabilities in K_2SeO_4 have been of considerable interest during the past two years. In the room-temperature (paraelectric) phase the crystal is orthorhombic with space group *Pnam* (D_{2h}^{16}).[2] At 129.5 K the crystal undergoes a displacive-type of structural phase transition into an incommensurate phase, as is evidenced by the presence of satellite peaks in x-ray[3] and neutron scattering[4] studies. Furthermore, neutron measurements show that this structural instability is driven by a soft phonon propagating with a wave vector $\vec{q}=\frac{1}{3}[(1-\delta)\vec{a}^*]$, where $\vec{a}^*$ is the first reciprocal-lattice vector along the [100] direction. As the crystal is cooled still further, δ decreases and vanishes abruptly at 93 K, when the crystal locks into a commensurate superstructure whose a axis is triple the size of that of the room-temperature phase. The structure of this new phase is also orthorhombic with space group $Pna2_1$ and the crystal acquires a spontaneous polarization along the c axis. Iizumi *et al.*[4] have provided an explanation for the appearance of this spontaneous polarization at the "lock-in" transformation by postulating a fourth-order anharmonic coupling between the soft mode and another mode of different symmetry which transforms in the same way as the electric polarization. Also, it is known from the dielectric measurements of Aiki *et al.*[5] that the spontaneous polarization of K_2SeO_4 below the "lock-in" transition is anomalously small. It follows from these observations that K_2SeO_4 should be classified as an improper ferroelectric according to the criteria provided by Dvorak.[6]

The present investigation had the following objectives:

(a) We wished to explore whether a rigid-ion model treated in the quasiharmonic approximation could be employed successfully to provide information on the nature of the structural instability in K_2SeO_4. Specifically, we wanted to identify those forces which were primarily responsible for the mode softening.

(b) We wished to understand how an incommensurate phase, such as those which occur in metallic charge-density-wave systems, could arise in an insulating crystal such as K_2SeO_4.

 ©1980 The American Physical Society

TABLE I. Prototypic atomic positions for K_2SeO_4 (*Pnam*).[a]

Prototype	x/a	y/b	z/c	Wyckoff designation
Se	0.2242	0.4200	$\frac{1}{4}$	$4(c)$
$K^{(1)}$	0.1705	0.0843	$\frac{1}{4}$	$4(c)$
$K^{(2)}$	−0.0057	−0.2905	$\frac{1}{4}$	$4(c)$
$O^{(1)}$	0.2931	0.3471	0.0271	$8(d)$
$O^{(2)}$	0.3024	−0.4356	$\frac{1}{4}$	$4(c)$
$O^{(3)}$	0.0126	0.4251	$\frac{1}{4}$	$4(c)$

[a]Reference 2.

(c) We wanted to explore the general question of structural instabilities in systems which are isomorphous with K_2SeO_4.

The organization of this paper is as follows. In Sec. II we discuss the static equilibrium conditions (SEC) which allow us to evaluate the first radial derivatives of the short-range potential. Section III deals with the vibrations of the free-selenate molecule. In Sec. IV we present the results of our calculations for the zone-center frequencies and give a comparison of the Raman-active frequencies with the measured values. In Sec. V we present complete sets of calculated dispersion curves for the [100] or Σ direction, in Sec. VI we show a detailed study of the soft branch, and in Sec. VII we discuss the displacement pattern for the soft mode. Section VIII is reserved for conclusions.

II. STATIC EQUILIBRIUM CONDITIONS

In its room-temperature phase K_2SeO_4 crystallizes with the orthorhombic space group *Pnam* having lattice parameters $a = 7.661 \pm 0.004$ Å, $b = 10.466 \pm 0.008$ Å, and $c = 6.003 \pm 0.003$ Å, as determined by Kalman *et al.*[2] There are four formula units (i.e., 28 atoms) per unit cell, and the prototypic coordinates of the atoms, as published in Ref. 2, are given in Table I. The structure can be visualized (see Fig. 1) as consisting of two distinct types of plane separated by half a lattice vector along the c axis, with the K^+ ions and the $(SeO_4)^{2-}$ tetrahedral groups embedded in each plane in the manner indicated.

The lattice-dynamical calculation was based on a rigid-ion model which was first developed by Boyer and Hardy[7] to study the lattice dynamics of gadolini-

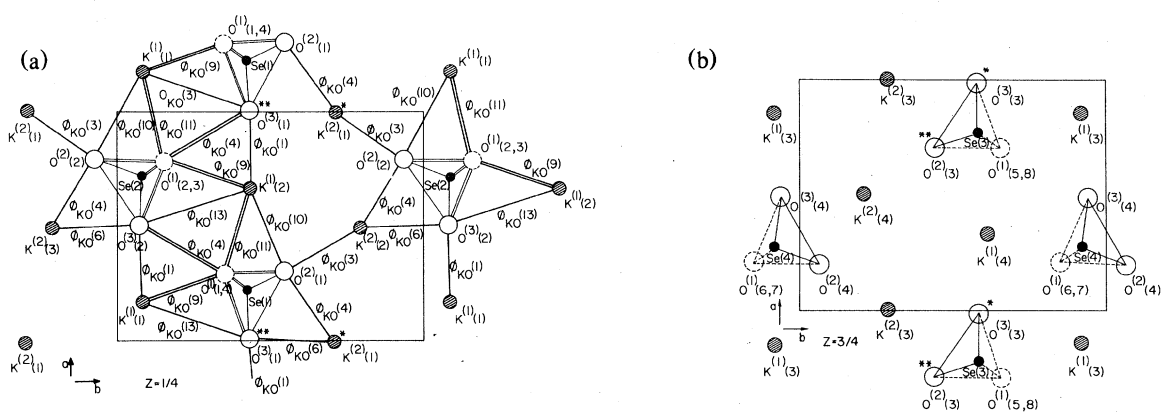

FIG. 1. Unit cell of K_2SeO_4 in the room-temperature phase showing the arrangements of atoms in the two distinct types of plane which are perpendicular to the c axis and separated by $\frac{1}{2}c$. The $O^{(1)}$ atoms, which are denoted by broken circles, lie outside these planes. (a) shows the interplanar bonds whose associated short-range potentials were considered in the lattice-dynamical model. The corresponding bonds in (b) may be obtained by symmetry. Double lines indicate pairs of bonds to $O^{(1)}$ atoms, which lie above and below the a-b plane. The asterisks label pairs of atoms in different planes whose short-range interactions critically influence the lattice instability. Two other such pairs are not shown in the figure.

um molybdate, $Gd_2(MoO_4)_3$. The short-range force-constant parameters were defined in terms of a central potential, and the ionic charge of the oxygen ions was treated as a variable parameter to allow for possible covalent bonding between oxygen and selenium ions within the selenate group. It was also assumed that the potassiums were completely ionized; thus the charge on the selenate radical was −2.

The dynamical matrix for an ionic crystal such as K_2SeO_4 consists of a long-range Coulomb term and a short-range overlap contribution. We calculated the former by the standard Ewald technique.[8] For central potentials, the latter is completely specified by the first and second radial derivatives of the potential for each of the close neighbor bonds included in the calculation. Table II lists the 32 shortest bonds and their associated potentials. In the following we describe how the first radial derivatives of the short-range potentials were determined from the equilibrium conditions for the static lattice.

For the lattice in its equilibrium configuration the internal force on each sublattice as well as the macroscopic stress along each of its principal axes must be zero. For complex crystals, such as K_2SeO_4, these conditions are not automatically satisfied by symmetry and can be formally expressed as an exact cancellation between Coulomb and short-range forces. These constitute the static equilibrium conditions (SEC), and are given by[9]

$$\sum_{kl}{}' \phi'(x(l,kk'))\frac{x_\alpha(l,kk')}{x(l,kk')} + F_\alpha(k') = 0 \qquad (1)$$

and

$$\frac{1}{2}\sum_{lkk'}{}' \phi'(x(l,kk'))\frac{x_\alpha(l,kk')x_\beta(l,kk')}{x(l,kk')} + f_{\alpha\beta} = 0 \ . \qquad (2)$$

Here $\vec{x}(l,kk')$ is the vector distance between the equilibrium position of the ion at site k in the origin unit cell and that of the ion at site k' in the lth unit cell and $\phi'(x(l,kk'))$ is the first radial derivative of the short-range potential between these ions evaluated at their equilibrium separation. $F_\alpha(k)$ and $f_{\alpha\beta}$ are the Coulomb counterparts of the first terms on the left-hand sides of Eqs. (1) and (2), respectively, and can be put into a rapidly convergent form using the Ewald technique. The full expressions for these are given in Ref. 9 and their values are completely specified by the ionic charges and coordinates.

It is readily seen that, given the ionic charges, Eqs. (1) and (2) can be used to determine the values of a set of ϕ''s from the calculated values of $F_\alpha(k)$ and $f_{\alpha\beta}$, provided the number of ϕ''s in the set is equal to the number of SEC. (Note that we use ψ' rather than ϕ' for intraselenate bonds.) For K_2SeO_4 there are 13 internal strain conditions, two from each of the five different symmetry species occupying c sites (Se, $K^{(1)}$, $K^{(2)}$, $O^{(2)}$, $O^{(3)}$), and three from the $O^{(1)}$ ions at d sites [superscripts on chemical symbols refer to symmetry species, while numbers on line with these symbols refer to atom numbers; e.g., $K^{(1)}(2)$ is the second potassium in the unit cell of the first symmetry species]. In addition there are three distinct

TABLE II. Listing of the non-Coulomb potentials for the 32 shortest bonds for K_2SeO_4. Potentials for bonds which are internal to a selenate molecular group are designated by ψ. Potentials marked with an asterisk act between atoms in adjacent planes.

Designation	Ion pair	Bond Length (Å)	Designation	Ion pair	Bond length (Å)
$\psi_{SeO}(1)$	Se-$O^{(3)}$	1.6219	$\phi_{KO}(10)$	$K^{(1)}$-$O^{(2)}$	3.2210
$\psi_{SeO}(2)$	Se-$O^{(2)}$	1.6257	$\phi_{KO}(11)$	$K^{(1)}$-$O^{(1)}$	3.2658
$\psi_{SeO}(3)$	Se-$O^{(1)}$	1.6282	$\phi_{KO}(12)$ *	$K^{(2)}$-$O^{(3)}$	3.3161
$\psi_{OO}(1)$	$O^{(2)}$-$O^{(1)}$	2.6397	$\phi_{OO}(1)$ *	$O^{(1)}$-$O^{(1)}$	3.3270
$\psi_{OO}(2)$	$O^{(2)}$-$O^{(3)}$	2.6561	$\phi_{OO}(2)$ *	$O^{(3)}$-$O^{(3)}$	3.3920
$\psi_{OO}(3)$	$O^{(1)}$-$O^{(3)}$	2.6598	$\phi_{SeK}(1)$	Se-$K^{(1)}$	3.4194
$\psi_{OO}(4)$	$O^{(1)}$-$O^{(1)}$	2.6760	$\phi_{OO}(3)$ *	$O^{(1)}$-$O^{(2)}$	3.4722
$\phi_{KO}(1)$	$K^{(1)}$-$O^{(3)}$	2.6227	$\phi_{SeK}(2)$	Se-$K^{(2)}$	3.5046
$\phi_{KO}(2)$ *	$K^{(2)}$-$O^{(1)}$	2.7375	$\phi_{SeK}(3)$	Se-$K^{(1)}$	3.5374
$\phi_{KO}(3)$	$K^{(2)}$-$O^{(2)}$	2.7859	$\phi_{SeK}(4)$	Se-$K^{(1)}$	3.5520
$\phi_{KO}(4)$	$K^{(2)}$-$O^{(2)}$	2.8067	$\phi_{OO}(4)$	$O^{(1)}$-$O^{(3)}$	3.5685
$\phi_{KO}(5)$ *	$K^{(2)}$-$O^{(1)}$	2.8224	$\phi_{OO}(5)$ *	$O^{(1)}$-$O^{(2)}$	3.6370
$\phi_{KO}(6)$	$K^{(2)}$-$O^{(3)}$	2.9798	$\phi_{SeK}(5)$	Se-$K^{(2)}$	3.6943
$\phi_{KO}(7)$ *	$K^{(1)}$-$O^{(1)}$	3.0013	$\phi_{OO}(6)$ *	$O^{(1)}$-$O^{(3)}$	3.7331
$\phi_{KO}(8)$ *	$K^{(1)}$-$O^{(2)}$	3.0159	$\phi_{KO}(13)$	$K^{(1)}$-$O^{(3)}$	3.7664
$\phi_{KO}(9)$	$K^{(1)}$-$O^{(1)}$	3.1996	$\phi_{OO}(7)$ *	$O^{(2)}$-$O^{(3)}$	3.8529

external strain conditions arising from the nonequivalence of the three principal axes of the orthorhombic structure. It is thus possible to determine 16 different ϕ''s from Eqs. (1) and (2) once we have fixed the selenium and oxygen charges. We found, during the course of our calculations, that these could best be determined during the fit to the Raman frequencies to be described later (see Sec. IV) and that the optimum values of the selenium and oxygen charges were $Z_{Se}=2$ and $Z_O=-1$.

From Table II we see that there are seven bonds internal to each SeO_4 molecular complex; three Se-O bonds and four O-O bonds. It would seem logical that the associated values of ψ' should constitute seven of these unknowns, however, in the room-temperature phase of K_2SeO_4, the SeO_4 groups are near-perfect tetrahedra.[2] As a result, when we tried to use the SEC to determine these values of ψ', the resultant equations were almost singular. This occurred because the force on a given oxygen ion due to the selenium ion acts almost along the same line as the resultant force due to the other three oxygen ions. To overcome this difficulty we followed the method used by Boyer and Fleury[10] and used $\psi'_{OO}(4)$ as a variable input parameter.

The next step was to decide which bonds external to the selenate group to use in the determination of ϕ' from the SEC. We initially included short-range interactions for all of the bonds shown in Table II, except that we excluded potassium-selenium bonds; we did so on the ground that short-range interactions for such bonds should be negligible as each selenium is well shielded by its surrounding tetrahedron of oxygens. Thus we had 26 unknowns and only 16 SEC to determine them. To reduce the number of unknowns we assumed a central potential of the Born-Mayer form for the potassium-oxygen interactions

$$\phi_{KO}(r)=\lambda\exp[-\alpha(r-r_0)] \quad , \tag{3}$$

where λ and α were to be determined, and r_0 was given some convenient value reasonably close to the potassium-oxygen bond lengths.

The Born-Mayer form expresses the 13 unknown values of ϕ'_{KO} in the SEC equations in terms of only two parameters. Thus we were left with a total of 15 unknowns to determine. There was an additional difficulty. Four of the internal strain conditions involved balancing Coulomb forces on potassium ions against sums of short-range potassium-oxygen forces. These last are completely determined by only two parameters; λ and α. Consequently, the SEC produced an overdetermined set of equations. We therefore left unbalanced the two small components of the Coulomb force on the $K^{(2)}$ ions. This procedure left us with 14 SEC; therefore we could determine only 14 unknown parameters and we thus set $\phi'_{OO}(7)$ to zero since this was associated with the longest bond considered. Thus we finally arrived at 14 unknowns and 14 SEC. These nonlinear equations were solved by the technique outlined by Boyer and Fleury,[10] which is very similar to algorithms found in standard textbooks on numerical analysis.[11] The results are shown in Table III. Both in this table and elsewhere in this paper force-constant parameters are given in units such that the absolute magnitude of the electronic charge is unity and the unit of length is 1 Å.

TABLE III. First radial derivatives of short-range forces, and Born-Mayer parameters.

Z_O		-1.0	
$\psi'_{OO}(4)$	-0.150		-0.300
λ	0.0216		0.0216
α	3.33		3.33
$\psi'_{SeO}(1)$	-0.122		0.287
$\psi'_{SeO}(2)$	-0.094		0.301
$\psi'_{SeO}(3)$	-0.078		0.329
$\psi'_{OO}(1)$	-0.159		-0.320
$\psi'_{OO}(2)$	-0.122		-0.286
$\psi'_{OO}(3)$	-0.150		-0.319
$\psi'_{OO}(4)$	-0.150		-0.300
$\phi'_{OO}(1)$	0.071		0.124
$\phi'_{OO}(2)$	-0.006		-0.006
$\phi'_{OO}(3)$	0.009		0.009
$\phi'_{OO}(4)$	0.008		0.008
$\phi'_{OO}(5)$	0.006		0.006
$\phi'_{OO}(6)$	0.010		0.010

The short-range forces between ions external to the selenate group are practically independent of $\psi'_{OO}(4)$ with one exception: $\phi'_{OO}(1)$. This potential derivative is associated with an interselenate bond between two $O^{(1)}$ ions which is parallel to the z axis and lies along the same line as the bond with which $\psi'_{OO}(4)$ is associated.

III. LATTICE DYNAMICS OF THE FREE SELENATE GROUP

X-ray studies[2] indicate that in K_2SeO_4 the distortion of the selenate complex from perfect tetrahedral coordination is very small. Therefore the force-constant parameters internal to the selenate group in K_2SeO_4 are not expected to be very different from the free-radical values. Consequently, an investigation of the lattice dynamics of the free-selenate radical was undertaken to provide additional information for our calculations on the lattice dynamics of K_2SeO_4.

The free-selenate radical is a tetrahedral unit with four O ions, each at one corner of the tetrahedron,

and an Se ion at the center. For a molecule having the symmetry of the tetrahedral point group T_d there are four vibrational modes. A nondegenerate A_1-type mode, a doubly degenerate E-type mode, and two triply degenerate T_2-type modes, all of which are Raman active, with the two T_2-type modes being infrared active as well. The four observed frequencies[12] are $\nu_1 = 833\ \mathrm{cm}^{-1}$, $\nu_2 = 335\ \mathrm{cm}^{-1}$, $\nu_3 = 875\ \mathrm{cm}^{-1}$, and $\nu_4 = 432\ \mathrm{cm}^{-1}$.

The theory of the normal modes of a molecule with tetrahedral coordination bonded by central forces is given by Herzberg.[13] The force-constant parameters in a harmonic calculation are expressed in terms of the first and second radial derivatives of the two independent central potentials; one for oxygen-oxygen bonds and one for oxygen-selenium bonds. We shall denote these derivates by θ' and θ''. There are only three independent parameters, namely, θ'_{OO}, θ''_{OO}, θ''_{SeO}. The vanishing of forces on the ions in their equilibrium configuration yields the relationship $\theta'_{\mathrm{SeO}} = -\sqrt{6}\theta'_{\mathrm{OO}}$.

The four vibrational frequencies are related to these parameters by the expressions[13]

$$4\pi^2\nu_1^2 = \frac{\theta''_{\mathrm{SeO}}}{m_{\mathrm{O}}} + 4\frac{\theta''_{\mathrm{OO}}}{m_{\mathrm{O}}} , \tag{4}$$

$$4\pi^2\nu_2^2 = \frac{\theta''_{\mathrm{OO}}}{m_{\mathrm{O}}} + \frac{\theta'_{\mathrm{OO}}}{l m_{\mathrm{O}}} , \tag{5}$$

$$4\pi^2(\nu_3^2 + \nu_4^2) = 2\frac{\theta''_{\mathrm{OO}}}{m_{\mathrm{O}}} + \frac{4m_{\mathrm{O}} + 3m_{\mathrm{Se}}}{3m_{\mathrm{O}}m_{\mathrm{Se}}}\theta''_{\mathrm{SeO}} + \frac{2(3m_{\mathrm{Se}} + 16m_{\mathrm{O}})}{3m_{\mathrm{O}}m_{\mathrm{Se}}}\frac{1}{l}\theta'_{\mathrm{OO}} \tag{6}$$

and

$$16\pi^4\nu_3^2\nu_4^2 = \frac{2(4m_{\mathrm{O}} + m_{\mathrm{Se}})}{3m_{\mathrm{Se}}m_{\mathrm{O}}^2} \times \left[\theta''_{\mathrm{OO}}\theta''_{\mathrm{SeO}} + 8\theta''_{\mathrm{OO}}\frac{\theta'_{\mathrm{OO}}}{l} + 5\theta''_{\mathrm{SeO}} \times \frac{\theta'_{\mathrm{OO}}}{l} - 8\left(\frac{\theta'_{\mathrm{OO}}}{l}\right)^2\right] , \tag{7}$$

where m_{O} and m_{Se} refer to the oxygen and selenium masses, respectively, and l is the length of the edge of the tetrahedron in the equilibrium configuration. The first three of these equations were used to determine the unknown parameters from the observed frequencies. In Table IV we show the contributions from the short-range overlap potential to these parameters when the ionic charge on oxygen, $Z_{\mathrm{O}} = -1$, the value determined by our lattice-dynamical calculations.

Since the selenate molecule does not distort very much in the crystal environment, the frequencies corresponding to the internal vibrations of the molecule are not changed by large amounts.[14,15] Hence the values of the short-range components of θ'' serve as good initial guesses for the values of ψ''_{SeO} and ψ''_{OO}. Additionally, the value of $\psi'_{\mathrm{OO}}(4)$, which was used as a variable input parameter in the SEC calculations, was initially set equal to the value determined from θ'_{OO}.

TABLE IV. Values of the short-range contributions to the force-constant parameters θ' and θ'' determined from the free SeO_4 vibrations for $Z_{\mathrm{O}} = -1$.

Z_{O}	θ''_{OO}	θ''_{SeO}	θ'_{OO}	θ'_{SeO}
−1.0	0.117	2.874	−0.481	0.769

IV. FREQUENCIES AT $\vec{q} = 0$

In this section we classify the zone-center normal modes by their symmetries and optical activities, set up the dynamical matrix in the limit as $\vec{q} \to 0$, partition this matrix into diagonal blocks which transform as the irreducible representations of the point symmetry group of the crystal, and finally describe the diagonalization of these symmetrized blocks to obtain the zone-center normal mode frequencies.

To conform with the notation of other workers on this system.[2–4,14,15] we define the crystal axes of K_2SeO_4 in its room-temperature phase to be such that the space group is *Pnam*. The character table for the group of the wave vector at the Γ point ($\vec{q} = 0$) is shown in Table V.

We performed a detailed group-theoretical analysis of the zone-center normal modes, and the results are shown in Table VI. The "internal" modes are those which are internal to the selenate molecular complex; the remaining modes are called "external" modes. We further classified the latter set according as to whether they involve vibrations or rotations of the selenate complexes, or translations of the crystal as a whole (the translations correspond to acoustic modes). This analysis is based on the correlation tables published by Fateley *et al.*[16] We verified these results by computing the multiplicity at each of the occupied sites of K_2SeO_4 using the subroutine BLOCDI published by Boyer[17]: These are shown in Table VII. The total multiplicity, which is given in the extreme right-hand column, was obtained by multiplying the entries in the two left-hand columns by the number of species which occupy sites of the corresponding symmetry and adding the results. For example, there are five different species which occupy c sites: Se,

TABLE V. Character table for the group of the wave vector at the Γ point.

	E	$C_2(z)$	$C_2(y)$	$C_2(x)$	i	$\sigma(xy)$	$\sigma(zx)$	$\sigma(yz)$		[a]
A_g	1	1	1	1	1	1	1	1		$xx(aa), yy(bb), zz(cc)$
B_{1g}	1	−1	1	−1	1	−1	1	−1	R_z	$xy(ab)$
B_{2g}	1	1	−1	−1	1	1	−1	−1	R_y	$xz(ac)$
B_{3g}	1	−1	−1	1	1	−1	−1	1	R_x	$yz(bc)$
A_u	1	1	1	1	−1	−1	−1	−1		
B_{1u}	1	−1	1	−1	−1	1	−1	1	T_z	
B_{2u}	1	1	−1	−1	−1	−1	1	1	T_y	
B_{3u}	1	−1	−1	1	−1	1	1	−1	T_x	

[a]Nonzero Raman polarizability tensor elements referred to both Cartesian and crystal axes.

$K^{(1)}$, $K^{(2)}$, $O^{(2)}$, and $O^{(3)}$, but only one at the d sites: $O^{(1)}$. Consequently the total multiplicity for the A_g symmetry is $5\times 2+1\times 3=13$. The total multiplicities for the irreducible representations shown in Table VII agree with those calculated from the correlation tables of Fateley *et al.*[16] which are listed in the right-hand column of Table VI.

The dynamical matrix at $\vec{q}=0$ is a real symmetric matrix of order 84. The Coulomb part, which was calculated by the Ewald method,[8] using as input the ionic charges and the crystal structure,[2] is not regular at $\vec{q}=0$; it depends on the direction of $\vec{q}$ as $\vec{q}\rightarrow 0$. To bypass this difficulty we computed the Coulomb terms for a very small value of $\vec{q}$ along the [100] (Σ) direction, which is the direction for which we eventually calculated the phonon dispersion curves.

The short-range contribution to the dynamical matrix is a function of the first and second radial derivatives of the short-range potentials. We obtained the former from the SEC, as described in Sec. II. We shall now describe how the latter were determined by fitting the calculated frequencies for $\vec{q}\simeq 0$ to those of the observed Raman-active modes. In order to start the calculations we needed some initial guesses for those parameters. For bonds internal to the selenate group we chose the values of ψ''_{SeO} and ψ''_{OO} given by θ''_{SeO} and θ''_{OO} for the appropriate value of Z_O. For external bonds the Born-Mayer form for the K-O potential determined both ϕ'_{KO} and ϕ''_{KO}. We found that, in addition to including the second derivatives of ϕ for potassium-oxygen bonds, it was essential to include second derivatives of ϕ for oxygen-oxygen bonds external to the selenate molecule.

The dynamical matrix thus constructed yields 84 eigenfrequencies, three of which correspond to the three acoustic modes and thus are approximately zero. We did not, however, diagonalize the full dynamical matrix. Such a procedure not only re-

TABLE VI. Symmetry classification of the zone-center normal modes for K_2SeO_4 in the *Pnam* structure.

D_{2h}	Vibr.	External modes rot.	Acoustic	Internal modes	Optical activity	Total
A_g	6	1	0	6	Raman	13
B_{1g}	6	1	0	6	Raman	13
B_{2g}	3	2	0	3	Raman	8
B_{3g}	3	2	0	3	Raman	8
A_u	3	2	0	3	···	8
B_{1u}	2	2	1	3	ir	8
B_{2u}	5	1	1	6	ir	13
B_{3u}	5	1	1	6	ir	13
Total	33	12	3	36		84

quires a large amount of computer time but also makes it impossible to classify the eigenfrequencies according to their symmetry species. Thus, initially, we block diagonalized the full dynamical matrix in such a manner that each block and its associated eigenvalues corresponded to the symmetry of one of the eight different irreducible representations for the Γ point. The order of a given block was given by the multiplicity of that particular irreducible representation. As a result, the largest of the matrices which we actually diagonalized was of order 13 and all eigenfrequencies were automatically associated with the appropriate symmetry. The initial block diagonalization was achieved by use of a unitary matrix $\vec{U}(\vec{q})$. This was done using the subroutine BLOCDI[17] which constructs symmetry basis vectors and generates the matrix $\vec{U}(\vec{q})$ using a projection operator. The input to this subroutine are the character table and the symmetry operations of the group of the wave vector $\vec{q}$. The dynamical matrix in its block-diagonalized form, $\vec{D}_B$, is then given by

$$\vec{D}_B(\vec{q}) = \vec{U}^+(\vec{q})\vec{D}(\vec{q})\vec{U}(\vec{q}) \ , \tag{8}$$

where $\vec{D}(\vec{q})$ is the full dynamical matrix for the chosen wave vector $\vec{q}$.

For very small values of $\vec{q}$ the part of the dynamical matrix which is regular as $\vec{q} \to 0$ has the same symmetry as the corresponding matrix at $\vec{q}=0$. It can thus be block diagonalized by a unitary matrix constructed using the symmetry basis vectors of the Γ point. If our small wave vector also lies along the Σ direction then the nonregular Coulomb part of the dynamical matrix is also diagonalized by this transformation. Since this was the case we could block diagonalize the total dynamical matrix using the transformation constructed for the Γ point and associate the resultant groups of eigenfrequencies with the symmetries of the irreducible representations at the Γ point. It should be noted that this is *not* true for an *arbitrary* small value of $\vec{q}$ and only holds for the Σ direction because the nonregular part of $\vec{D}$ is invariant under the transformation $x \to -x$.

TABLE VII. Multiplicities associated with the occupied sites of K_2SeO_4 in the *Pnam* structure.

	Occupied Sites (Wyckoff) (*c*)	(*d*)	Total
A_g	2	3	13
B_{1g}	2	3	13
B_{2g}	1	3	8
B_{3g}	1	3	8
A_u	1	3	8
B_{1u}	1	3	8
B_{2u}	2	3	13
B_{3u}	2	3	13

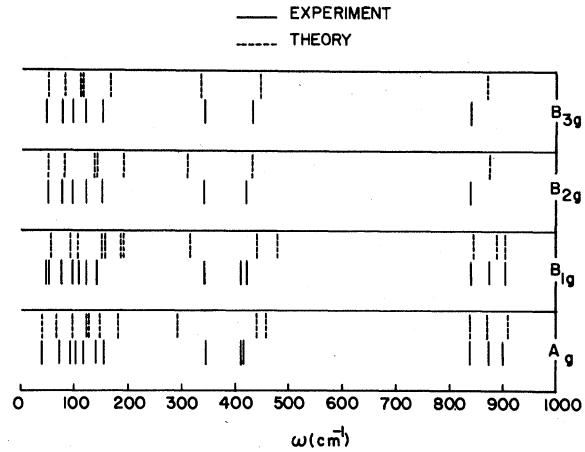

FIG. 2. Observed and calculated Raman frequencies for K_2SeO_4 at 130 K. The observed values are taken from Ref. 18. In every experimental spectrum more lines are seen than are predicted by group theory and we have identified as genuine first-order lines only the most intense lines in any region whose frequencies are those shown in the figure. This criterion reduces the number of lines to the group theoretical value.

The positions of the calculated zone-center Raman active frequencies are shown in Fig. 2 along with those of the observed frequencies.[18] The remaining calculated zone-center frequencies are given in Table VIII. Note that the B_{1u}, B_{2u}, and B_{3u} modes are infrared active. However experimental measurements of the appropriate spectra do not appear to exist.

At this point a brief comment on the experimental

TABLE VIII. Calculated odd-parity zone-center mode frequencies for K_2SeO_4 at 130 K.

A_u (cm^{-1})	B_{1u} (cm^{-1})	B_{2u} (cm^{-1})	B_{3u} (cm^{-1})
16.80	0.00	0.00	0.00
74.67	53.03	67.14	94.13
102.55	92.00	95.79	133.57
136.10	128.21	113.09	140.30
155.23	162.43	152.87	150.92
286.44	299.76	177.13	159.67
400.67	396.18	191.30	219.75
874.08	874.94	349.69	296.30
		398.10	452.30
		438.14	495.95
		852.61	875.20
		878.18	902.85
		904.93	913.61

TABLE IX. First and second radial derivatives of the short-range potentials.

Short-range potential	First radial derivative	Second radial derivative
$\psi_{SeO}(1)$	−0.122	3.0000
$\psi_{SeO}(2)$	−0.094	3.2500
$\psi_{SeO}(3)$	−0.078	3.2000
$\psi_{OO}(1)$	−0.159	0.1160
$\psi_{OO}(2)$	−0.121	0.1160
$\psi_{OO}(3)$	−0.150	0.1160
$\psi_{OO}(4)$	−0.150	0.1160
$\phi_{KO}(1)$	−0.067	0.2223
$\phi_{KO}(2)$	−0.046	0.1517
$\phi_{KO}(3)$	−0.039	0.1291
$\phi_{KO}(4)$	−0.036	0.1205
$\phi_{KO}(5)$	−0.034	0.1143
$\phi_{KO}(6)$	−0.020	0.0507 (0.0677)
$\phi_{KO}(7)$	−0.019	0.0550 (0.0630)
$\phi_{KO}(8)$	−0.018	0.0504 (0.0600)
$\phi_{KO}(9)$	−0.010	0.0386 (0.0326)
$\phi_{KO}(10)$	−0.009	0.0503 (0.0303)
$\phi_{KO}(11)$	−0.008	0.0201 (0.0261)
$\phi_{KO}(12)$	−0.007	0.0241 (0.0221)
$\phi_{KO}(13)$	−0.001	0.0020 (0.0000)
$\phi_{OO}(1)$	0.071	0.0050
$\phi_{OO}(2)$	−0.006	0.0150
$\phi_{OO}(3)$	0.009	0.0250
$\phi_{OO}(4)$	0.008	0.0400
$\phi_{OO}(5)$	0.006	−0.0030
$\phi_{OO}(6)$	0.010	−0.0200
$\phi_{OO}(7)$	0.000	−0.0152

papers of Fawcett *et al.*[14] and Wada *et al.*[15] is in order. Our nomenclature for the irreducible representations: B_{1g}, B_{2g}, B_{3g}, B_{1u}, B_{2u}, and B_{3u} is the same as that used in Ref. 4, but does not agree with the designations used in Refs. 14 and 15. Proper connection can however be established for the Raman-active modes if one expresses the elements of the Raman-polarizability tensor with respect to the crystal axes *a*, *b*, and *c*. This is done explicitly in the last column of Table V.

In Table IX we list the values of the first and second radial derivatives of the short-range potentials. These are the parameters which we used to calculate the zone-center frequencies as well as the dispersion curves which we shall discuss in Sec. V. The value of the oxygen ionic charge used was −1.

We now turn to a discussion of the zone-center Raman-active frequencies and consider first those modes whose frequencies lie in the range 300–900 cm^{-1}. These correspond to the internal modes of the selenate and are derived from the free-molecular vibrations (see Sec. III). As is to be expected, these frequencies are almost entirely determined by parameters which are internal to the selenate group, i.e., ψ'_{SeO}, ψ''_{SeO}, ψ'_{OO}, and ψ''_{OO}. In particular the frequencies in the range 800–900 cm^{-1} are most strongly dependent upon $\psi''_{SeO}(1)$, $\psi''_{SeO}(2)$, and $\psi''_{SeO}(3)$; it can be seen that the values for these are fairly close to the free-molecular value shown in Table IV. The frequencies in the 300–500 cm^{-1} range correspond to ν_2(=335 cm^{-1}) and ν_4(=432 cm^{-1}) for the free-selenate ion. These are primarily affected by the first and second derivatives of intraselenate short-range oxygen-oxygen potentials. Of these $\psi'_{OO}(4)$ was used as a variable parameter in the SEC equations. We found that $\psi'_{OO}(4) = -0.150$ gave best overall agreement between theory and experiment. In spite of the fact that $\psi'_{OO}(4) = -0.481$ for the free molecule, we chose to use $\psi'_{OO}(4) = -0.150$ in our calculations as giving a better overall fit to the observed frequencies, including those of the external modes in the 0–200 cm^{-1} range. The agreement with experiment in the 300–500 cm^{-1} range is not particularly good, but this may be due to the fact that we have no angle bending forces in our model of the selenate group.

It was during this part of the fitting procedure that the value of $Z_O = -1$ was determined to be the optimum value. Any lower *(more negative)* value led to difficulties in fitting the high-frequency section of the Raman spectrum, while any larger *(more positive)* value would seem to imply an implausible degree of covalent bonding in the selenate radical.

For the external frequencies we found that using Born-Mayer predicted values for all the ϕ''_{KO}'s did not yield good agreement with experiment at very low frequencies. To remove this discrepancy we found that it was necessary to change the values of $\phi''_{KO}(6)$ to $\phi''_{KO}(13)$ from those given by the Born-Mayer potential. The degree of change can be seen from Table IX where the latter are shown in parentheses.

V. PHONON DISPERSION FOR $\vec{q}$ ALONG THE Σ DIRECTION

The group of the wave vector along the [100] or Σ direction is the group of all operations which leave the wave vector invariant. These operations are the identity, a twofold rotation about the *x* axis, and reflections in the *x-z* and *x-y* planes. The character table for this group is shown in Table X. If we now compare this character table with that for the Γ point group given in Table V we obtain the compatibility relations between the irreducible representations of these two groups. These are shown in Table XI; also shown are the corresponding relations with the irreducible representations of the zone-boundary *X* point group. The multiplicities of the Σ and *X* representations are then obtained by using the compatibility relations in conjunction with multiplicities of

TABLE X. Character table for the group of the wave vector along Σ.

C_{2v}	E	C_{2x}	σ_{xy}	σ_{zx}		
Σ_1	1	1	1	1	T_x	xx,yy,zz
Σ_2	1	1	−1	−1	R_x	yz
Σ_3	1	−1	1	−1	$T_z;R_y$	xz
Σ_4	1	−1	−1	1	$T_y;R_z$	xy

the Γ representations given in Table VI. We then have

$$\Sigma:\ 26\Sigma_1 \oplus 16\Sigma_2 \oplus \Sigma_3 \oplus 26\Sigma_4\ ,$$

$$X:\ 26X_1 \oplus 16X_2\ .$$

The two representations at the X point are each doubly degenerate, and we have verified the multiplicities for the Σ direction by an independent calculation using Boyer's subrouting BLODCI.[17]

Complete sets of phonon dispersion curves for the Σ direction, calculated using the parameters of Table IX, are presented in Figs. 3 to 6. The dynamical matrix for modes of each symmetry for a given $\vec{q}$ was obtained by a block-diagonalization procedure, based on the group of the wave vector, similar to that used for calculations at the zone center. The most significant result of these calculations is shown in Fig. 5 where we see that there is a pronounced softening of an optical branch of Σ_2 symmetry in the neighborhood of $\vec{q}=0.3\vec{a}^*$. This is the soft branch which has been observed by Iizumi *et al.*[4] by inelastic neutron scattering. This branch is degenerate at the X point with a transverse-acoustic branch of Σ_3 symmetry which has displacements along the c axis of the crystal. These results are in general accord with the findings of the neutron measurements.[4]

TABLE XI. Compatibility relations among the irreducible representations of the groups of the wave vector, at the Γ point, along the Σ direction, and at the X point.

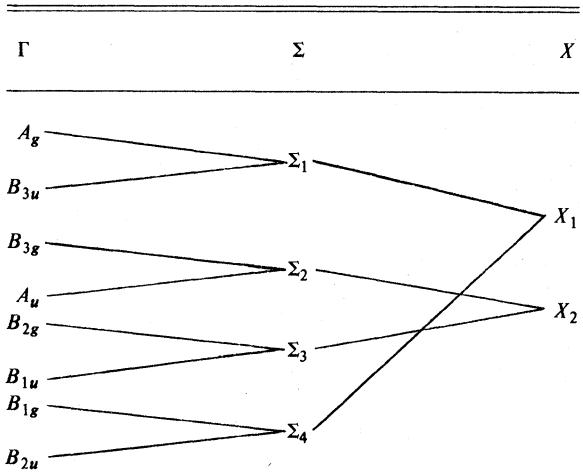

VI. STUDIES OF THE SOFT MODE

Our calculations are based on a harmonic lattice model and are thus not capable of reproducing the temperature dependence of phonon frequencies. Nevertheless it is known that in insulating crystals, such as K_2SeO_4, mode softening results from cancellation between two competing forces: Coulomb and short range. Thus, we performed a systematic study of the effect of varying the second derivatives of the various short-range potentials, and thereby the balance between Coulomb and short-range forces, on the soft Σ_2 branch. We found that only those deriva-

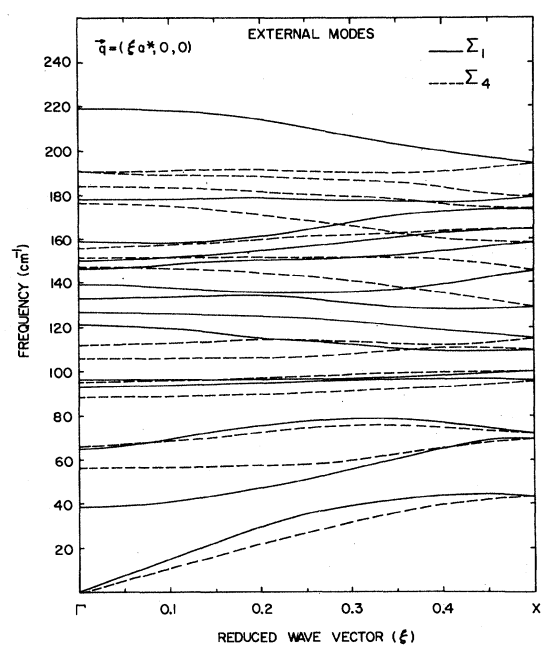

FIG. 3. Phonon dispersion curves for the Σ_1 and Σ_4 external vibrations.

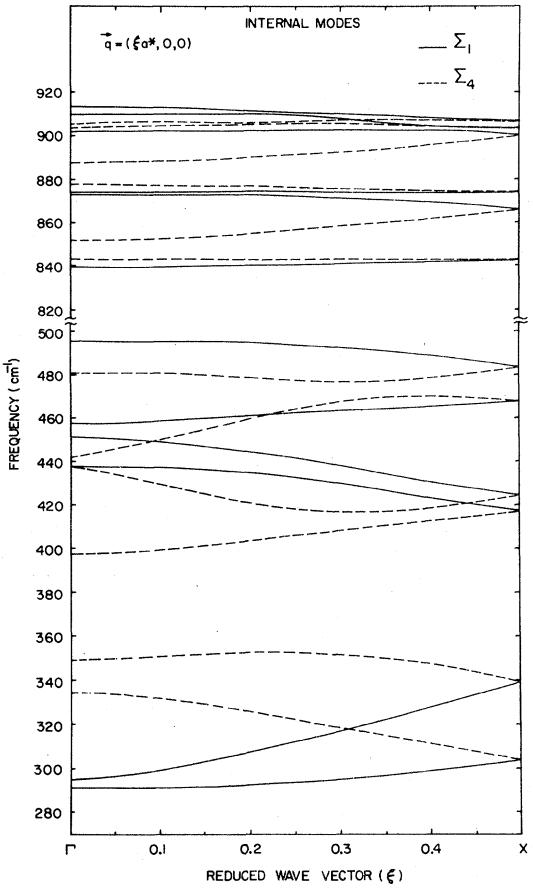

FIG. 4. Phonon dispersion curves for the Σ_1 and Σ_4 internal vibrations.

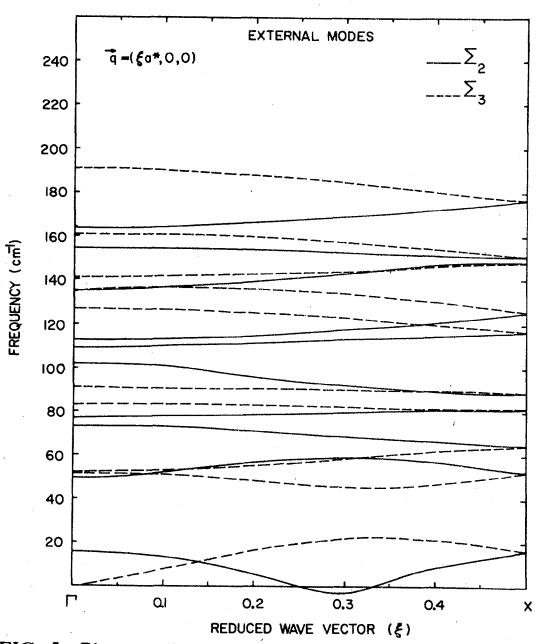

FIG. 5. Phonon dispersion curves for the Σ_2 and Σ_3 external vibrations.

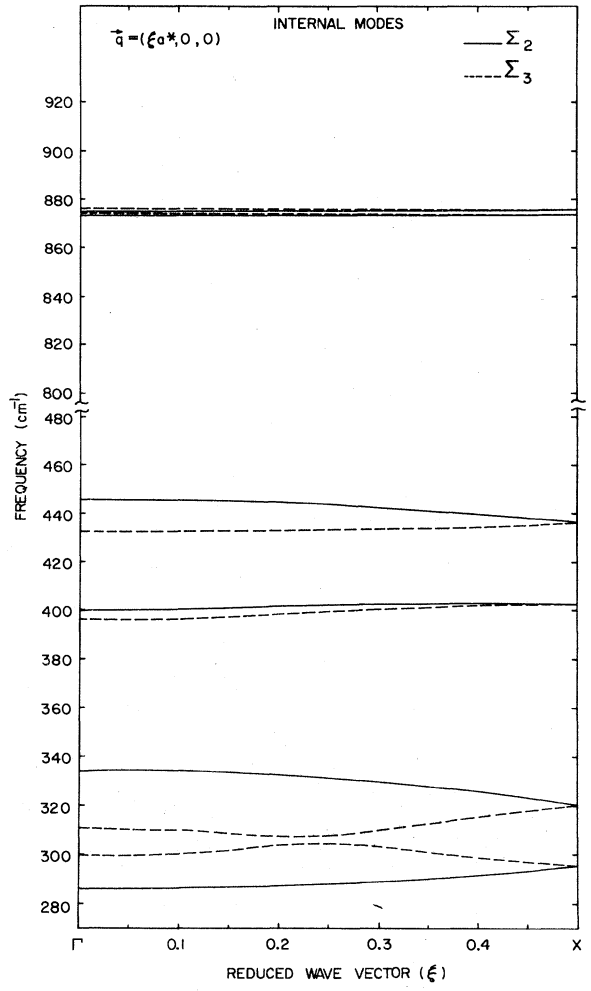

FIG. 6. Phonon dispersion curves for the Σ_2 and Σ_3 internal vibrations.

tives associated with bonds which have components along the c axis of the crystal affect this branch. These are mainly bonds between atoms in two different planes (see Fig. 1). This is to be expected because the displacements associated with a mode of Σ_2 symmetry are mostly along the c axis.

Of the various interplanar derivatives the ones which affect the soft branch most strongly are $\phi''_{KO}(8)$, $\phi''_{KO}(12)$, $\phi''_{OO}(6)$, and $\phi''_{OO}(7)$ [bonds KO(12) and OO(7) are indicated in Fig. 1]. Specifically the frequency of the soft Σ_2 branch at the zone center, which corresponds to a mode of A_u symmetry, is most sensitive to changes in $\phi''_{KO}(12)$. However, while the whole of this Σ_2 branch is similarly sensitive to changes in this parameter, our calculations also show that, especially for $\vec{q} \gtrsim 0.3\,\vec{a}^*$, it is much more sensitive to changes in $\phi''_{OO}(7)$. The reason for this can be deduced from Fig. 1; there we see that the KO(12) bond has a very small component along

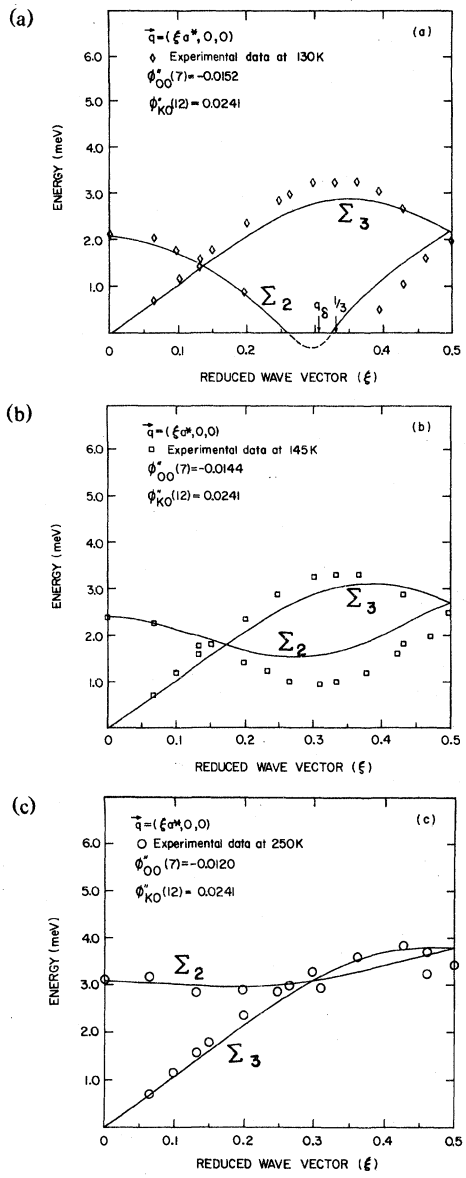

FIG. 7(a) Calculated dispersion curves for the Σ_2 soft branch and the associated Σ_3 acoustic branch at 130 K. The portion of the Σ_2 branch indicated by the broken line below the horizontal axis has imaginary frequencies. Also shown are the experimental points from Ref. 4. (b) Calculated dispersion curves for the Σ_2 soft branch and the associated Σ_3 branch at 145 K. Also shown are the experimental points from Ref. 4. (c) Calculated and observed (Ref. 4) dispersion curves for the Σ_2 soft branch and the associated Σ_3 branch at 250 K. Also shown are the experimental points from Ref. 4.

the Σ direction (a axis), while the OO(7) bond has a substantial component. It thus follows that contributions to the dynamical matrix from KO(12) bonds will be almost independent of $\vec{q}$, while those from OO(7) bonds will be strongly $\vec{q}$ dependent for $\vec{q}$ vectors along the [100] direction. In our calculations we have simulated the effect of varying the temperature by altering the value of $\phi''_{OO}(7)$.

In Fig. 7(a) we show the soft Σ_2 branch and the associated Σ_3 branch calculated with the parameters given in Table IX. Also shown are the neutron scattering results[4] for 130 K. Both the calculated branches are in good agreement with the neutron data. In particular, the Σ_2 branch has imaginary frequencies (shown by the dotted curve) for a range of wave vectors with a minimum at $\vec{q} \simeq 0.3\vec{a}^*$.

The results of our simulation of the effect of temperature on the Σ_2 and Σ_3 branches are shown in Figs. 7(b) and 7(c) where we present results appropriate to 145 and 250 K, respectively. The calculated dispersion curves were obtained by adjusting the value of $\phi''_{OO}(7)$ to be such that the calculated frequency of the Σ_2 mode at the zone center (the A_u mode) was in very close correspondence with the experimental value. No other parameters were changed. It can be seen that the Σ_2 branch hardens very rapidly for small changes in $\phi''_{OO}(7)$.

We mentioned earlier that the softening of a phonon frequency in an insulating crystal is the result of a cancellation between Coulomb and short-range forces. In order to demonstrate this cancellation explicitly for K_2SeO_4 we followed a procedure first used by Yoshimitsu[19] for $SrTiO_3$ and decomposed the eigenfrequencies into Coulomb and short-range contributions.

The eigenvalue problem for lattice dynamics can be expressed as

$$D_{ij}e_j^r = \omega_r^2 e_i^r \ , \tag{9}$$

where D_{ij} are the components of the dynamical matrix, e_j^r are the eigenvector components, and ω_r^2 is the square of the eigenfrequency. Now one can write

$$D_{ij} = D_{ij}^C + D_{ij}^s \ , \tag{10}$$

where D_{ij}^C and D_{ij}^s refer to the Coulomb and short-range parts of the dynamical matrix. We now define two sets of frequencies ω_s and ω_C by

$$(e_i^r)^* D_{ij}^C (e_j^s) = \omega_C^2(rs) \tag{11a}$$

and

$$(e_i^r)^* D_{ij}^s (e_j^s) = \omega_s^2(rs) \ . \tag{11b}$$

From Eqs. (9) and (10) and the orthonormality of eigenvectors it follows that

$$\omega_C^2(rs) + \omega_s^2(rs) = \begin{cases} \omega^2, & \text{for } r = s, \\ 0, & \text{for } r \neq s \end{cases} \ . \tag{12}$$

In Fig. 8 we show the diagonal elements of the ω^2 matrices in Eq. (12) for the Σ_2 soft branch and the Σ_3 acoustic branch plotted as a function of wave vector.

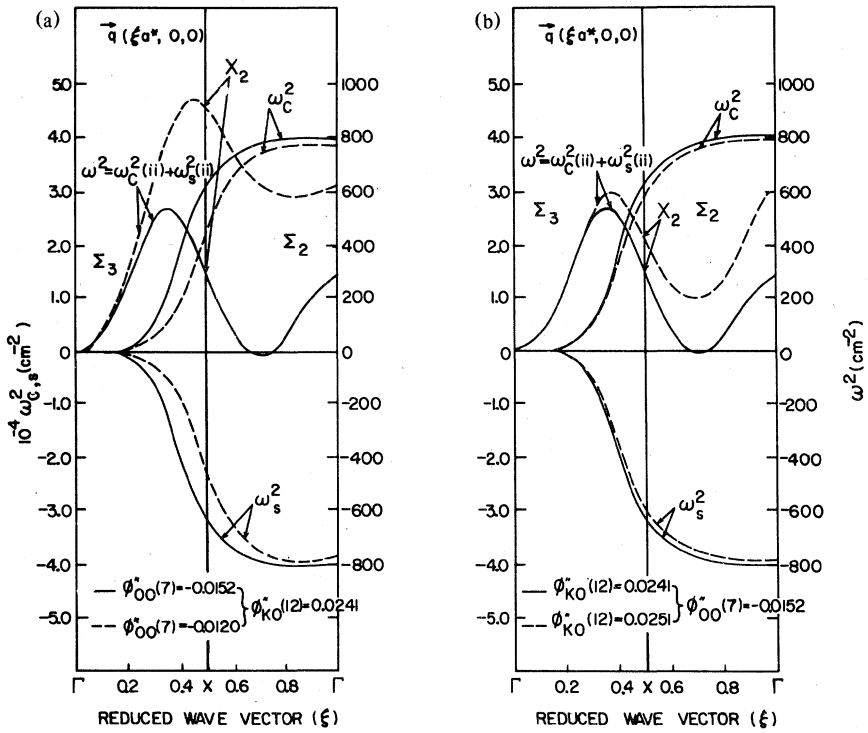

FIG. 8. Plots of frequency squared as a function of wave vector, in the extended zone scheme, for the Σ_2 soft branch and the Σ_3 acoustic branch showing the decomposition into Coulomb and short-range components. The left panel shows the effect of varying $\phi''_{OO}(7)$, whereas the right panel shows the effect of changing $\phi''_{OO}(12)$. The scales on the right refer to square of the true frequency ω^2, whereas the scales on the left refer to the Coulomb and short-range contributions, namely, $\omega_C^2(rr)$ and $\omega_s^2(rr)$, respectively. In both figures the observed position of the instability is indicated by a vertical bar on the central horizontal axis.

The plot is made using the extended zone scheme, consequently the Σ_2 optical branch appears as a continuation of the Σ_3 acoustic branch.

The results shown in Fig. 8(a) correspond to two different values of $\phi''_{OO}(7)$ for a fixed value of $\phi''_{KO}(12)$, whereas those shown in Fig. 8(b) correspond to two separate values of $\phi''_{OO}(12)$ for a constant value of $\phi''_{OO}(7)$.

A detailed discussion of these results for different values of $\phi''_{OO}(12)$ has already been published,[1] and we will not repeat it here. There are, however, some quantitative differences between the results presented here and those published in Ref. 1. These discrepancies are a result of our having used different model parameters in the two calculations. The parameters used in Ref. 1 were partially determined by fitting the Raman data of Fawcett *et al.*[14] and Wada *et al.*[15] Recent measurements by Massa and Ullman[18] have revealed certain discrepancies in the earlier measurements. The model parameters used in the present calculations were derived from a fit to these new Raman data.[18]

It is also apparent from Fig. 8 that the frequencies of the Σ_2 branch become imaginary when the contributions from the *destabilizing* short-range forces dominate those from the *stabilizing* Coulomb forces and that there is nothing special about the wave vector at which the instability occurs. It is thus not surprising that the lattice makes a transition to an incommensurate phase. Moreover, as the actual frequencies are the square roots of small differences between very large numbers, one can infer that the balance between stabilizing and destabilizing forces is very delicate in the K_2SeO_4 structure.

VII. SOFT-MODE EIGENVECTORS AND DISPLACEMENTS

Within the harmonic approximation the αth component of the displacement of the kth atom in the lth unit cell is given by[9]

$$u_\alpha(lk) = \frac{1}{(Nm_k)^{1/2}} \sum_{j\vec{q}} e_\alpha(k\,|\,\vec{q}\,j)\,Q(\vec{q}\,j)\exp\{i[\vec{q}\cdot\vec{x}(lk)+\Delta(\vec{q}\,j)]\} \ . \tag{13}$$

Here $e_\alpha(k\,|\,\vec{q}j)$ are the eigenvector components for the jth branch of wave vector $\vec{q}$, $Q(\vec{q}j)$ is the corresponding normal coordinate, m_k is the mass of the kth atom, $\vec{x}(lk)$ locates the equilibrium position of the atom (l,k), $\Delta(\vec{q}j)$ is an arbitrary phase factor, and N is the number of unit cells. From Eq. (13) we can extract the displacement due to a given mode, and for the soft mode we write this

$$\xi_\alpha(lk) \propto \frac{1}{\sqrt{m_k}}\{S_\alpha(k\,|\,\vec{q}_s\,\Sigma_2)Q\exp[i\beta(lk)+i\Delta]+S_\alpha^*\,(k\,|\,\vec{q}_s\,\Sigma_2)Q^*\exp[-i\beta(lk)-i\Delta]\}\ , \tag{14}$$

where S_α is the appropriate component of the soft-mode eigenvector,

$$\beta(lk)=\vec{q}_s\cdot\vec{x}(lk) \tag{15}$$

and $\vec{q}_s$ is the wave vector of the soft mode. If we set $Q\propto 1+i$, we obtain

$$\xi_\alpha(lk) \propto \frac{1}{\sqrt{m_k}}R_\alpha(k\,|\,\vec{q}_s\,\Sigma_2)\{\cos[\beta(lk)+\theta_\alpha(k\,|\,\vec{q}_s\,\Sigma_2)+\Delta]-\sin[\beta(lk)+\theta_\alpha(k\,|\,\vec{q}_s\,\Sigma_2)+\Delta]\}\ , \tag{16}$$

where

$$S_\alpha(k\,|\,\vec{q}_s\,\Sigma_2)=R_\alpha(k\,|\,\vec{q}_s\,\Sigma_2)\exp[i\theta_\alpha(k\,|\,\vec{q}_s\,\Sigma_2)]\ . \tag{17}$$

If we follow the phase convention of Ref. 4 we have

$$S_\alpha^*\,(k\,|\,\vec{q}_s\,\Sigma_2)=S_\alpha(\bar{k}\,|\,\vec{q}_s\,\Sigma_2)\ , \tag{18}$$

where k and $\bar{k}$ are related to each other by the inversion operation. Equation (18) implies that

$$\theta_\alpha(k\,|\,\vec{q}_s\,\Sigma_2)=-\theta_\alpha(\bar{k}\,|\,\vec{q}_s\,\Sigma_2)\ . \tag{19}$$

Equation (19) was not satisfied by the phase angles of eigenvectors computed by our diagonalization routine. Consequently we defined new phase angles

$$\theta'_\alpha(k\,|\,\vec{q}_s\,\Sigma_2)=\theta_\alpha(k\,|\,\vec{q}_s\,\Sigma_2)+\Delta \tag{20}$$

and then attempted to find a single value of Δ such that these new phase angles satisfied Eq. (18). In this we were successful. Thus the arbitrary phase angle Δ is determined in accord with the convention of Ref. 4. When this value of Δ is used in Eq. (16) the resultant displacements are directly comparable with those of Ref. 4.

The soft-mode eigenvector components are shown in Table XII. (The phase angles quoted do not include Δ.) The z components of the associated displacements are shown in Fig. 9, together with those which we calculated from the experimentally determined eigenvectors.[4] Also shown in Fig. 9 are calculated displacements which correspond to the stiffened up soft mode at 250 K [see Fig. 7(c)]. The two sets of experimental displacements are identical and belong to the soft mode at 130 K. The theoretical results show the displacements for the potassium atoms together with those of the centers of mass of the selenate groups. We make no similar direct comparisons for the various oxygen displacements since the experimental determination was based on the assumption that the selenate tetrahedra are rigid units.

In both sets of displacements shown in Fig. 9, we scaled the magnitudes of the calculated displacements to be such that there is exact agreement between theoretical and experimental displacements for the $K^{(2)}(1)$ atom. These are marked by asterisks in the figure. Although the detailed agreement between the calculated and experimental displacements is rather poor, one can see that the calculated selenate displacements are generally smaller than the potassium displacements; this is in agreement with experiment.

Figure 9 also shows that stiffening the soft mode by changing $\phi''_{00}(7)$ from -0.0152 to -0.0120 produces a considerable alteration in the displacement pattern.

One serious discrepancy between theory and experiment is that the observed $K^{(1)}$ displacements are generally larger than the $K^{(2)}$ displacements. The calculated displacements have the opposite behavior. This discrepancy can be traced back to the calculated eigenvectors (see Table XII); in these the amplitudes (R_z) for $K^{(2)}$ are larger than those for $K^{(1)}$.

VIII. SUMMARY AND CONCLUSIONS

We have presented the results of calculations on the lattice dynamics of K_2SeO_4 at 130 °K. The dispersion curve for the low-frequency Σ_2 branch [Fig. 7(a)] shows a softening of modes with wave vectors $\vec{q}\sim 0.3\,\vec{a}^*$ in agreement with experiment.[4] The slope of the Σ_3 acoustic branch for small wave vectors and its overall shape are also in good agreement with the observed results. An attempt to simulate the observed temperature dependence of these two dispersion curves by changing the parameter $\phi''_{00}(7)$ produced good agreement with experimental results obtained at 145 and 250 K [Figs. 7(b) and 7(c)]. The most significant disagreement between theory and experiment in the last two figures is that the calculated frequencies are slightly higher than the experimental frequencies near the zone boundary. It is, however, striking that variation of this single short-range force constant reproduces the observed temperature dependence of the two branches so well.

TABLE XII. Soft-mode eigenvectors.

k	$S_x(k\|\vec{q}_s\,\Sigma_2)$ R_x	θ_x (rad)	$S_y(k\|\vec{q}_s\,\Sigma_2)$ R_y	θ_y (rad)	$S_z(k\|\vec{q}_s\,\Sigma_2)$ R_z	θ_z (rad)
Se(1)	0	0	0	0	0.1463	0.2096
Se(2)	0	0	0	0	0.1463	−2.9320
Se(3)	0	0	0	0	0.1463	−1.7795
Se(4)	0	0	0	0	0.1463	1.3621
$K^{(1)}(1)$	0	0	0	0	0.1074	1.4768
$K^{(1)}(2)$	0	0	0	0	0.1074	−1.6648
$K^{(1)}(3)$	0	0	0	0	0.1074	−3.0466
$K^{(1)}(4)$	0	0	0	0	0.1074	0.0950
$K^{(2)}(1)$	0	0	0	0	0.1728	2.6063
$K^{(2)}(2)$	0	0	0	0	0.1728	−0.5353
$K^{(2)}(3)$	0	0	0	0	0.1728	2.1070
$K^{(2)}(4)$	0	0	0	0	0.1728	−1.0346
$O^{(2)}(1)$	0	0	0	0	0.2288	0.6323
$O^{(2)}(2)$	0	0	0	0	0.2288	−2.5093
$O^{(2)}(3)$	0	0	0	0	0.2288	−2.2022
$O^{(2)}(4)$	0	0	0	0	0.2288	0.9394
$O^{(3)}(1)$	0	0	0	0	0.2582	−0.7101
$O^{(3)}(2)$	0	0	0	0	0.2582	2.4315
$O^{(3)}(3)$	0	0	0	0	0.2582	−0.8598
$O^{(3)}(4)$	0	0	0	0	0.2582	2.2818
k	$S_x(k\|\vec{q}_s\,\Sigma_2)$ R_x	θ_x (rad)	$S_y(k\|\vec{q}_s\,\Sigma_2)$ R_y	θ_y (rad)	$S_z(k\|\vec{q}_s\,\Sigma_2)$ R_z	θ_z (rad)
$O^{(1)}(1)$	0.1455	1.6655	0.1080	0.4391	0.0353	1.4833
$O^{(1)}(2)$	0.1455	1.6655	0.1080	−2.7025	0.0353	−1.6583
$O^{(1)}(3)$	0.1455	−1.4761	0.1080	0.4391	0.0353	−1.6583
$O^{(1)}(4)$	0.1455	−1.4761	0.1080	−2.7025	0.0353	1.4833
$O^{(1)}(5)$	0.1455	−0.0938	0.1080	1.1326	0.0353	−3.0532
$O^{(1)}(6)$	0.1455	−0.0938	0.1080	−2.0090	0.0353	0.0884
$O^{(1)}(7)$	0.1455	3.0478	0.1080	1.1326	0.0353	0.0884
$O^{(1)}(8)$	0.1455	3.0478	0.1080	−2.0090	0.0353	−3.0532

Decomposition of the squares of the frequencies for the soft branch into Coulomb and short-range contributions shows that the occurrence of an incommensurate phase in potassium selenate and its isomorphs is a very likely possibility. Moreover, we have examined the manner in which the balance changes as two of the short-range force constants are increased (see Fig. 8; cf. Fig. 7). In both cases the soft Σ_2 branch hardens rapidly and one would thus expect the transition temperature to decrease as stress is applied, as was found to be the case experimentally.[1] However, this statement is based on the implicit assumption that ϕ'' increases with decreasing length for both KO(12) and OO(7) bonds. While the Born-Mayer form used for K-O potentials ensures that this is true for KO(12) bonds, we have no similar guarantee for OO(7) bonds. However, since Table IX shows a general decrease of ϕ'' with length for both K-O and O-O bonds it is plausible to argue that both stiffen (ϕ'' increases) as the crystal is stressed.

The agreement between experiment and our theoretical results is certainly not perfect. This is not to be expected considering the simplicitly of our model, which was imposed upon us by the structural complexity of the crystal. Disagreement between theory and experiment is particularly marked for the displacements associated with the soft mode. It is possible that this is not entirely due to defects in our model but may also be attributed, in part, to the effect of anharmonicity on the experimental determination of these displacements. Near the transition temperature the crystal is expected to be very anharmonic, and the mode coupling, which leads to improper ferroelectricity in the system below 93 °K, may well be significant at 130 K. It is thus possible that the

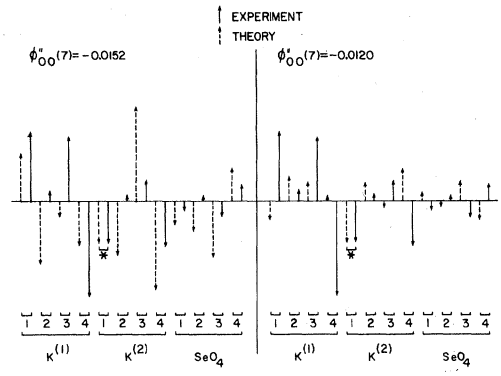

FIG. 9. Observed (Ref. 4) and calculated displacements along the c axis associated with the soft mode ($\vec{q}_s = 0.3\vec{a}^*$). The calculated displacements on the left-hand side are those of the soft mode at 130 K, whereas those on the right-hand side are those of the same mode on the 250 K dispersion curve. The observed displacements for both sets correspond to the soft mode at 130 K. Pairs marked with asterisks are those for which the magnitudes of the calculated displacements have been fitted to the observed values at 130 °K.

experimentally determined soft-mode displacements could reflect this coupling.

In spite of its shortcomings, our present rigid-ion model provides much insight into the origin and nature of the structural instability in potassium selenate. Using only structural and Raman data, we have been able to construct a version of the model capable of predicting the incommensurate structural instability and have been able to identify which of the short-range forces have the most critical influence on this instability. Finally, we have been able to use this knowledge to predict successfully the stress dependence of the transition temperature.

ACKNOWLEDGMENT

We are grateful to Dr. L. L. Boyer, Professor F. G. Ullman, and Dr. Q. Kim for many useful discussions. We are particularly indebted to Dr. Boyer for much guidance during the early stages of this investigation. This work was supported by the United States Army Research Office under Grant No. DAAG 29-77-G-0008.

---

*Now at Xerox Corporation, Xerox Square, Rochester, N.Y. 14644.

† To whom all correspondence should be addressed.

[1]M. S. Haque, J. R. Hardy, Q. Kim, and F. G. Ullman, Solid State Commun. 27, 813 (1978).

[2]A. Kálmán, J. S. Stephens, and D. W. J. Cruickshank, Acta Crystallogr. Sect. B 26, 1451 (1970).

[3]N. Ohama, Mater. Res. Bull. 9, 283 (1974).

[4]M. Iizumi, J. D. Axe, G. Shirane, and K. Shimaoka, Phys. Rev. B 15, 4392 (1977).

[5]K. Aiki, K. Hukuda, and O. Matumura, J. Phys. Soc. Jpn. 26, 1064 (1969).

[6]V. Dvorák, Ferroelectrics 7, 1 (1974).

[7]L. L. Boyer and J. R. Hardy, Phys. Rev. B 8, 2205 (1973).

[8]L. L. Boyer, Phys. Rev. B 9, 2684 (1974).

[9]L. L. Boyer and J. R. Hardy, Phys. Rev. B 7, 2886 (1973).

[10]L. L. Boyer and P. A. Fleury, Phys. Rev. B 9, 2693 (1974).

[11]B. Carnahan, H. A. Luther, and J. O. Wilkes, *Applied Numerical Methods,* (Wiley, New York, 1969), p. 308.

[12]K. Nakomoto, *Infrared Spectra of Inorganic and Coordination Compounds,* 3rd ed. (Interscience, New York, 1970), p. 142.

[13]G. Herzberg, *Infrared and Raman Spectra of Polyatomic Molecules* (Van Nostrand, New York, 1945), p. 165.

[14]V. Fawcett, R. J. B. Hall, D. A. Long, and V. N. Sankaranarayanan, J. Raman Spectrosc. 2, 629 (1974); 3, 229 (1975).

[15]M. Wada, A. Sawada, Y. Ishibashi, and Y. Takagi, J. Phys. Soc. Jpn. 42, 1229 (1977).

[16]W. G. Fateley, F. R. Dollish, N. T. McDevitt, and F. F. Bentley, *Infrared and Raman Selection Rules for Molecular and Lattice Vibrations* (Interscience, New York, 1972), p. 203.

[17]L. L. Boyer, J. Comp. Phys. 16, 167 (1974).

[18]N. Massa and F. G. Ullman (private communication). These data, shown in Fig. 2, differ in certain important respects from those of Refs. 14 and 15. Details are to be published later.

[19]K. Yoshimitsu, Prog. Theor. Phys. 54, 583 (1975).